

## Mechanisms of North Atlantic Wintertime Sea Surface Temperature Anomalies

MARTINA M. JUNGE\*

*Atmospheric, Oceanic, and Planetary Physics, University of Oxford, Oxford, United Kingdom*

THOMAS W. N. HAINE

*Earth and Planetary Sciences, The Johns Hopkins University, Baltimore, Maryland*

(Manuscript received 12 January 2001, in final form 20 June 2001)

### ABSTRACT

The authors address the question: What are the oceanic mechanisms that control North Atlantic sea surface temperature (SST) anomalies? The approach is to examine the sensitivity dynamics of a non-eddy-resolving North Atlantic Ocean general circulation model (GCM) using its adjoint. The adjoint GCM yields the sensitivity of end-of-winter SSTs to the prior ocean state and prior air-sea forcing over a seasonal cycle. Diagnosis of the sensitivity results identifies the oceanic mechanisms involved in controlling SST anomalies. The most effective way to alter SST is to change the local, contemporaneous air-sea heat flux. Wind stress and freshwater perturbations are ineffective over one year. Upstream, wintertime heat flux anomalies can cause SST fluctuations in the following winter but heat flux anomalies during summer weakly affect subsequent end-of-winter SSTs. The dominant mechanism is the end-of-winter detrainment of warmer or colder water and its subsequent entrainment downstream into the mixed layer the next winter. This process is more effective in the midlatitude and subpolar North Atlantic where deep winter mixed layers occur, than in the tropical-subtropical regions, which are characterized by a shallow mixed layer and a weak seasonal cycle. Mean-flow advection in the seasonal thermocline of the North Atlantic Current is moderately important in the subpolar gyre. Dynamical mechanisms, such as planetary waves and anomalous currents, are much less important over one year. The GCM results indicate that internal ocean anomalies forced by remote heat fluxes do affect SST variability. But, overall, contemporaneous winter heat flux anomalies are 3–30 times more effective at causing SST anomalies than heat flux anomalies from the previous winter. The loss of sensitivity to prior air-sea fluxes suggests that North Atlantic SST fluctuations are thus primarily a response to local, recent forcing.

### 1. Introduction

Predictability of winter temperature and precipitation over the northeast Atlantic Ocean and western Europe has become a tantalizing possibility in recent years. A key quantity to understand is the sea surface temperature (SST), and its fluctuations, which seem potentially influential for the ensuing atmospheric evolution (Latif et al. 2000; Venzke et al. 1999). Analyses of observed and modeled SST anomalies show persistence and coherent propagation over several winters (Sutton and Allen 1997; Gordon et al. 2000). The extent to which the North Atlantic atmospheric circulation drives these perturbations and how sensitive it is to them is still unclear. Nevertheless, coupled air-sea feedback mechanisms are

natural candidates to account for this type of itinerant low-frequency variability as the dominant oceanic time-scales are well-matched to the periods of interest. Here, we investigate aspects of these mechanisms focusing on the oceanic processes that influence SST variability.

Perhaps the most successful paradigm of midlatitude SST variability is the stochastic climate model of K. Hasselmann and C. Frankignoul (Hasselmann 1976; Frankignoul and Hasselmann 1977; Frankignoul 1985). Their idea recognizes the essential role the upper-ocean mixed layer plays as a heat capacitor whose large thermal inertia smoothes rapid variation in air-sea heat fluxes arising from tropospheric weather. The simple model for SST persistence includes a local negative feedback of heat flux on SST that damps anomalies with a time-scale of the order of 3 months (Frankignoul et al. 1998). Despite its simplicity, this stochastic model is remarkably successful in accounting for the statistical properties of real fluctuations.

Nevertheless, a striking feature of some midlatitude SST anomalies is their persistence from one winter to the next (Alexander and Deser 1995; Watanabe and Kimoto 2000). Clearly, processes exist that allow co-

\* Current affiliation: Istituto Nazionale di Geofisica e Vulcanologia, c/o ISAO-CNR, Bologna, Italy.

Corresponding author address: Dr. Martina M. Junge, Istituto Nazionale di Geofisica e Vulcanologia, c/o ISAO-CNR, via Gobetti 101, 40129 Bologna, Italy.  
E-mail: martina@traviata.imga.bo.cnr.it

herent signals to survive much longer than the stochastic-model damping timescale. This persistence might be provided by low-frequency power in the air–sea heat fluxes. James and James (1989) point out that long periods naturally exist in the atmospheric general circulation, for example. Alternatively, interactions between the mixed layer and the oceanic interior could account for the memory of SST anomalies. Several possibilities arise including exchange of fluid with the seasonal and permanent pycnocline, anomalous advective transport, and propagation of remotely generated waves.

Recent studies to unravel the importance of these various mechanisms have focused on statistical analyses of climatological datasets or output from coupled general circulation models (GCMs). When interpreting observations of such closed, interacting systems it is notoriously difficult to attribute the cause and effect of different mechanisms. Instead, the analyses are typically restricted to correlations that merely indicate mutual variability. Here, we have used the adjoint sensitivity method (Cacuci 1981; Errico 1997) that identifies causal chains. The great advantage of using an adjoint GCM is that these sensitivities are dynamically based and do not rely on statistical correlations. This approach allows us to quantify local and remote sensitivity of North Atlantic winter SST anomalies to (i) prior interior ocean temperatures, and (ii) prior atmospheric fluxes. Analysis of the sensitivity dynamics allows identification of linear oceanic mechanisms that control SST persistence from one winter to the next. Our overall goal is to understand and quantify the causal oceanic mechanisms that may account for the observed interannual persistence of SST anomalies. Our specific focus here is to understand the role of the seasonal cycle.

The article is organized as follows. The basis of the adjoint sensitivity method is explained in section 2. The ocean GCM is described in section 3 and the results of our numerical experiments are in section 4. The implications of our findings for the role of the ocean in low-frequency midlatitude climate variability are discussed in section 5.

## 2. Sensitivity analysis

We now give an overview of the adjoint sensitivity analysis used here. Further details may be found in Errico (1997) and the articles cited therein. Marotzke et al. (1999) and van Oldenborgh et al. (1999) have also applied the adjoint technique to questions of ocean circulation. Those readers who are familiar with adjoint theory in the present context can skip to section 3.

Consider the evolution of the general nonlinear system with state vector  $\Psi$

$$\frac{d\Psi}{dt} = L(\Psi). \quad (1)$$

Here, the tendency of the state is given by the nonlinear operator  $L$  (dependent on  $\Psi$ ) acting on  $\Psi$ . The elements

of the state vector comprise the different physical fields of interest discretized appropriately over space. In our case of the primitive equations of large-scale ocean circulation,  $\Psi$  consists of the three-dimensional flow, the temperature, salinity, and sea surface elevation. Given suitable initial and boundary data, (1) can be integrated to yield the evolution of  $\Psi$ .

Now consider how the trajectory through phase space differs when some aspect of the system is altered (e.g., when the air–sea heat fluxes are changed):

$$\frac{d}{dt}(\Psi + \Delta\Psi) = L'(\Psi + \Delta\Psi), \quad (2)$$

where  $\Delta\Psi$  is the resulting difference between the perturbed and unperturbed state vectors. In this case, the altered system evolves under a different nonlinear operator  $L'$  because the forward trajectory has itself changed. Physically, one can regard (2) as involving extra mechanisms that are not active in (1); namely, interactions between the basic state and the perturbation ( $\Psi$  and  $\Delta\Psi$ ) and interactions between the perturbation and itself ( $\Delta\Psi$  and  $\Delta\Psi$ ). For the chaotic large-scale ocean circulation, the difference in trajectories,  $\Delta\Psi$ , grows exponentially at first, reflecting the sensitive dependence on the exact initial and boundary conditions that apply. This divergence of trajectories ceases when the perturbation self-interactions are large enough to be of primary significance.

For small perturbations  $\delta\Psi$ , however, this wave–wave process can be neglected and the linearized system evolves according to

$$\frac{d\delta\Psi}{dt} = \mathbf{A}\delta\Psi, \quad (3)$$

where the matrix  $\mathbf{A} = \partial L/\partial\Psi$  is the linearized dynamical operator, or Jacobian, corresponding to  $L$ . The solution to this equation may be written

$$\delta\Psi(T) = \mathbf{G}(t, T)\delta\Psi(t), \quad (4)$$

using the forward-propagator matrix (or Green's function)  $\mathbf{G}$  to evolve the perturbation from time  $t$  to time  $T$ . In this tangent-linear system, the physical processes responsible for the (small) changes  $\delta\Psi$  can only arise from interactions between the perturbations and the basic state  $\Psi$ . There are no longer any wave–wave mechanisms and the wave–mean-flow interactions that remain are governed by a linear operator (3).

The tangent-linear system describes how a (small) perturbation in the basic state evolves with time. The linearity of the tangent-linear equations also allows a straightforward interpretation of this perturbation in terms of familiar linear mechanisms such as passive advection and wave dynamics. As such, this theory is ideal for determining the future impacts of small changes to the system. In the present context we are more interested in the sensitivity of the current state to earlier perturbations in the system. In other words, we also need

to understand what combination of physical processes brought about the current state, that is, what mechanisms are responsible for setting the current SST. The key to understanding this type of sensitivity is the system that is adjoint to (3) (Errico 1997).

The mathematical origin of the adjoint operator lies in the definition of an inner product that defines the projection of one state on another. The inner product yields a scalar-valued function of the state,  $J$ , and it is the sensitivity of this scalar that the adjoint system produces. In our case,  $J$  is the area-averaged SST at the end of winter. Denoting the inner product with angled brackets ( $\langle \cdot, \cdot \rangle$ , essentially an integral over all space),

$$J = \langle \Psi(T), \mathcal{K} \rangle \quad (5)$$

is the scalar function of the final state of the system at time  $T$  where the sensitivity kernel function  $\mathcal{K}$  defines the area-averaging operation over the region of interest. We require the sensitivity of  $J$  in the sense that

$$\delta J = \langle \nabla_t J, \delta \Psi(t) \rangle, \quad (6)$$

where  $\nabla_t J$  is the sensitivity at the earlier time  $t$ . Given knowledge of this sensitivity and the perturbation  $\delta \Psi$  we are able to calculate the change in  $J$  at time  $T$  using this formula.

To find the sensitivity  $\nabla_t J$  we exploit a general property of the inner product,

$$\langle \mathbf{u}, \mathcal{L}\mathbf{v} \rangle = \langle \mathbf{v}, \mathcal{L}^\dagger \mathbf{u} \rangle, \quad (7)$$

where  $\mathbf{u}$  and  $\mathbf{v}$  are arbitrary vectors,  $\mathcal{L}$  is a linear operator, and  $\mathcal{L}^\dagger$  is the corresponding adjoint operator. Equation (7) is the bilinear identity or Green's identity (Lanczos 1961; Morse and Feshbach 1953). Essentially, it guarantees the existence, and defines, the adjoint operator  $\mathcal{L}^\dagger$  (the transpose of the Jacobian) corresponding to the (forward) operator  $\mathcal{L}$ . When  $\mathbf{u} = \mathcal{K}$ ,  $\mathbf{v} = \delta \Psi(t)$ , and  $\mathcal{L} = \mathbf{G}(t, T)$ , the bilinear identity reads

$$\langle \mathcal{K}, \mathbf{G}(t, T) \delta \Psi(t) \rangle = \langle \delta \Psi(t), \mathbf{G}^\dagger(T, t) \mathcal{K} \rangle. \quad (8)$$

Hence,

$$\nabla_t J = \mathbf{G}^\dagger(T, t) \mathcal{K} \quad (9)$$

or, in other words, the sensitivity is given by the adjoint propagator  $\mathbf{G}^\dagger(T, t)$  evolving the sensitivity kernel backward to the earlier time  $t$ . In our case, the kernel is a temperature average over a specific surface region. Using this kernel as a source for the adjoint propagator yields the sensitivity to averaged SST we require.

The adjoint system arises directly from the properties of the tangent-linear system. As the tangent-linear problem only involves linear processes the corresponding adjoint system is also linear. Indeed, the familiar mechanisms of (small amplitude) wave dynamics and passive transport are reflected in the adjoint problem. There are typically just differences of sign between the tangent-linear and adjoint differential operators. This property has important implications for the discussion of physical mechanisms below. (i) We can discuss the solutions of

the adjoint system using the usual ideas of waves and tracer transport, although the time order of events may be somewhat unfamiliar. In other words, understanding the sensitivity dynamics requires a readjustment of perspective but uses the same (linear) physical ideas used to understand the forward dynamics. (ii) The mechanisms excluded in this discussion are nonlinear self-interactions that eventually cause sufficient divergence of trajectories so that the perturbed state no longer resembles the basic state. The time taken for this exponential growth phase depends on the (finite time) Lyapunov exponents of the tangent-linear system (defined by the singular values of  $\mathbf{G}$ ) and the initial perturbation (Smith et al. 1997; Farrell and Ioannou 1996; Palmer 1995). The corresponding sensitivities, derived from the adjoint, exhibit exponential growth backward in time for the same reasons (Lea et al. 2000). So, to the extent that we seek to understand the linear causality involved in these perturbations [sometimes called predictability of the first kind; Palmer (1996)] our attention is focused on the tangent-linear and adjoint systems. In this paper, we calculate adjoint sensitivities of a non-eddy-resolving GCM that does not exhibit chaotic dynamics. Non-chaotic nonlinearity may still be important, however, and we explore this possibility in section 4e.

In practice, we focus on the sensitivity of SST to prior oceanic conditions and forcing. Specifically, we estimate the relative importance of (remotely forced) internal ocean mechanisms compared to local (in space and time) forcing on SST. By including a relaxation term in the surface ocean heat budget, we capture the main features of the stochastic model of air-sea interaction. The implication for the adjoint model is an exponential loss of sensitivity integrating backward in time—the stochastic model causes a loss of memory of earlier SST conditions. As we will see, other ocean mechanisms are influential indicated by the departure from exponential damping of sensitivity.

### 3. The Hamburg North Atlantic model and adjoint

The ocean general circulation model used in this study is the Hamburg Ocean Primitive Equation (HOPE) model (Wolff et al. 1997) adapted for the Atlantic domain north of 40°S (A. Sterl 1999, personal communication). This primitive equation GCM has been used extensively in studies of climate variability in coupled mode (Grötzer et al. 1998; Latif and Barnett 1996). The prognostic variables are the three-dimensional velocity field, sea surface elevation, temperature, and salinity. The North Atlantic ocean model extends from 40°S–80°N and 100°W–20°E. The grid points are organized on an Arakawa E grid, which is a staggered composition of two grids overlaying each other in such a way that the “even” mesh is shifted half a grid step in both eastern and northern direction in relation to the “odd” mesh. The resolution of each of these grids is 1.4° in latitude and longitude with 20 levels in the vertical (the upper

10 levels represent the upper 300 m of the water column). Realistic topography and coastline are implemented. At the northern and southern boundaries, temperature and salinity are relaxed toward the Levitus (1982) climatology over the whole water column. The Mediterranean outflow is also parameterized. A constant climatological distribution of sea ice is applied. Linearly interpolated climatological monthly mean fields have been used to force the circulation. The forcing fields derive from the Hellermann and Rosenstein (1983) wind stress, Esbensen and Kushnir (1981) heat fluxes and solar radiation, and Jaeger (1976) precipitation minus Esbensen and Kushnir (1981) evaporation fields. In ice-free areas, surface temperature  $T$  is relaxed toward the Levitus (1982) climatology  $T_{\text{clim}}$  such that the restoring heat flux is given by  $\lambda(T - T_{\text{clim}})$  where  $\lambda$  is  $40 \text{ W m}^{-2} \text{ } ^\circ\text{C}^{-1}$ . This heat flux implies a timescale for relaxation of SST anomalies, or loss of sensitivity, of about two months (for a water column 40 m deep). A similar relaxation is applied to sea surface salinity with a timescale of 30 days. These forcing fields drive an annual cycle that is designed to capture the main features of North Atlantic seasonal climatology—the GCM shows little interannual variability. Assessing the effects of realistic low-frequency oceanic variations on sensitivity mechanisms is an interesting issue but beyond our present scope.

Initial conditions for the 20-yr spinup run are taken from the Levitus (1982) hydrography with the model starting from a state of rest. The winter and summer model circulation at 50 m after 20 yr is shown in Fig. 1. We see that the model Gulf Stream on the western boundary in the North Atlantic exhibits maximum speeds of  $0.6 \text{ m s}^{-1}$  and shows the familiar problem of separating too far north from the North American coast, at about  $40^\circ\text{N}$ . East of  $50^\circ\text{W}$  the Gulf Stream extension separates into three branches: the North Atlantic Current, the Azores Current, which eventually feeds the sluggish subtropical gyre circulation, and the recirculating branch into the Sargasso Sea. Surface currents in the Labrador Current reach  $0.10\text{--}0.15 \text{ m s}^{-1}$  in winter. In the tropical Atlantic the North Brazil Current reaches speeds of  $1.2 \text{ m s}^{-1}$  in August. The model North Equatorial Counter Current (NECC) peaks in August with surface speeds of  $0.5 \text{ m s}^{-1}$  and is not present at all in February. The South Equatorial Current also shows speeds of up to  $0.5 \text{ m s}^{-1}$ .

The depth of the mixed layer plays a crucial role in determining the seasonal heat loss and gain by the ocean. In winter, when surface heat loss and strong winds tend to deepen the mixed layer, subsurface temperatures influence SSTs to some degree. In summer, when ocean heat gain stabilizes the water column, the mixed layer becomes shallow and subsurface water masses are shielded from atmospheric influence and may retain some memory of previous winter conditions. In the Hamburg model, the mixing near the sea surface depends on the local Richardson number, which mea-

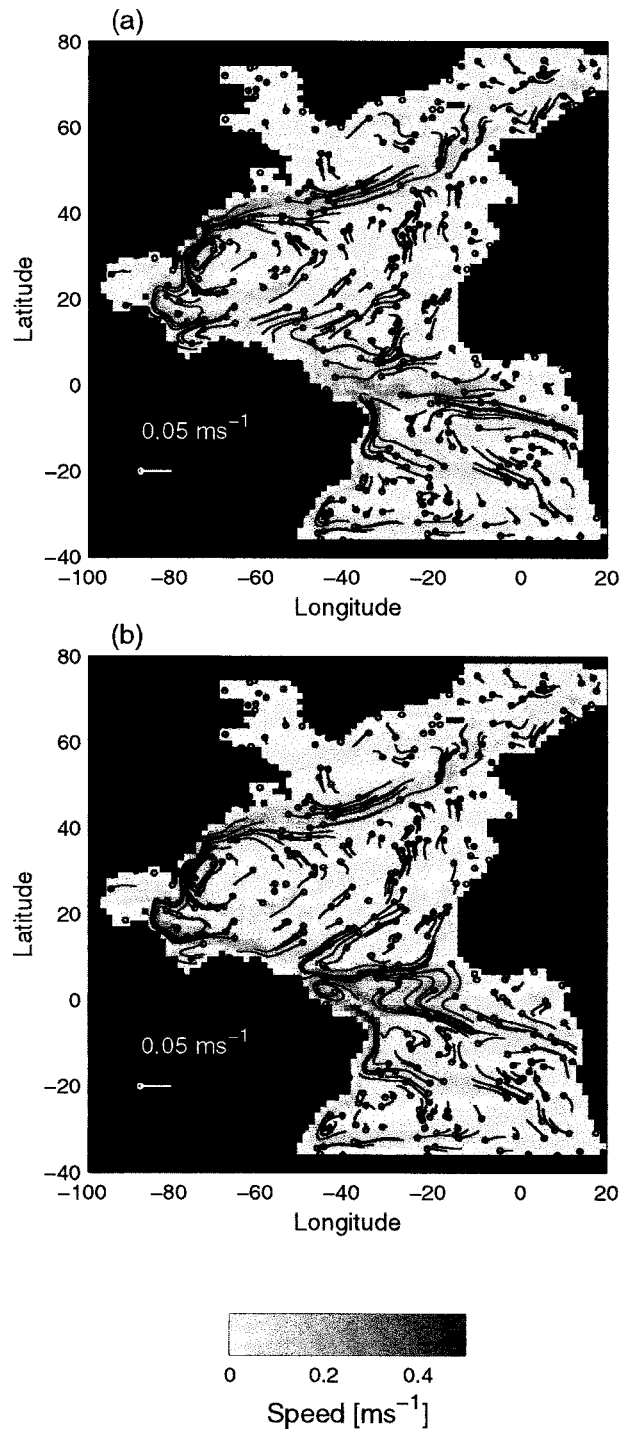


FIG. 1. Speed ( $\text{m s}^{-1}$ ) at 50-m depth on (a) 1 Feb and (b) 1 Aug after a 20-yr spinup integration. Streamlines, whose length indicates the horizontal displacement along the instantaneous streamline, are shown for 180 days starting from the small circles. The equivalent length of a  $0.05 \text{ m s}^{-1}$  current is also shown.

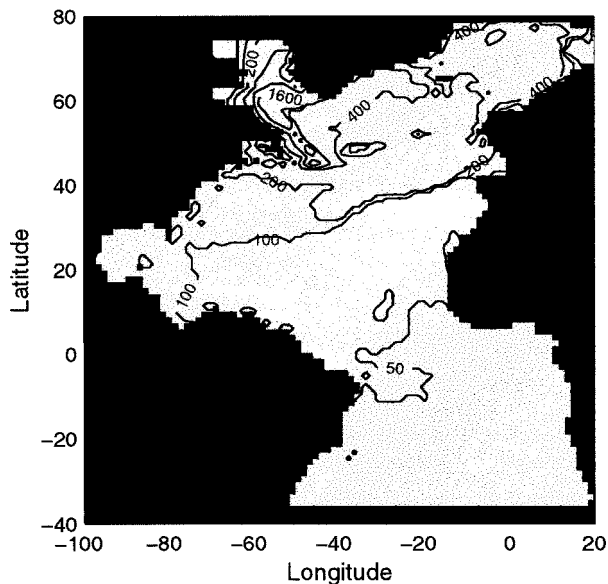


FIG. 2. Mixed layer depth (m) on 1 Apr estimated as the depth at which the temperature is  $0.5^{\circ}\text{C}$  less than the surface temperature. Contours are plotted at 50, 100, 200, 400, 800, 1600, and 3200 m.

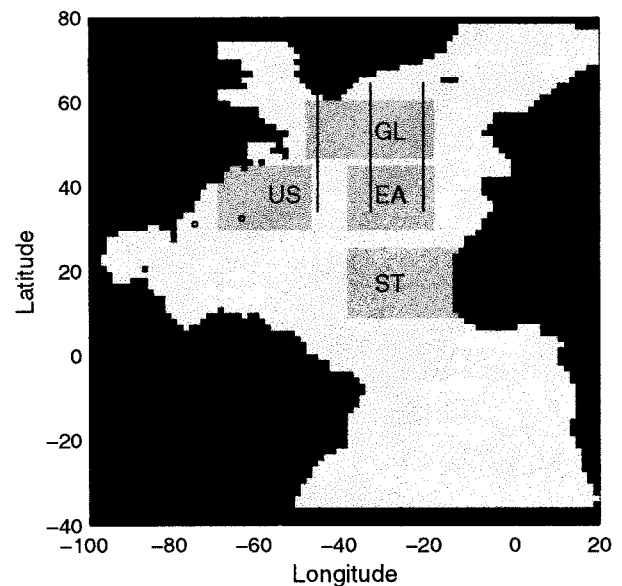


FIG. 3. Model domain showing the four areas over which 1 year 2 SST is averaged to define the scalar function,  $\mathcal{J}$ . The small circles indicate the station locations in Fig. 5 and the solid lines show the locations of three sections shown in Fig. 7.

sures the combined effect of buoyancy forcing and vertical current shear. Although this is a rather ad hoc parameterization, comparison with observations shows that the model produces a homogeneous upper layer of realistic depth. To estimate the mixed layer depth we use the depth at which the deviation of temperature from the surface value equals  $0.5^{\circ}\text{C}$ . This depth is shown in Fig. 2 for 1 April. The mixed layer is shallowest in the tropical and eastern subtropical North Atlantic with values between 50 and 100 m, and becomes progressively deeper toward the northwest. High values are also found in the northeastern corner of the domain, in the convection areas of the Greenland and Norwegian Seas. This picture is in reasonable agreement with mixed layer depth inferred from observations, for example, Marshall et al. (1993, cf. their Fig. 4a).

The adjoint model was derived from a version of the HOPE hybrid coupled model used for studies of the delayed-action oscillator theory of the El Niño–Southern Oscillation (van Oldenborgh et al. 1999). This code was then adapted to the North Atlantic configuration used here. An automatic source-to-source cross compiler, the tangent linear and adjoint model compiler, was used extensively to help generate the adjoint software (Giering and Kaminski 1998; Marotzke et al. 1999).

#### 4. SST sensitivity results

In this section we describe sensitivity experiments with the Hamburg GCM and adjoint. The focus is on the importance of prior air–sea heat fluxes in controlling SST, and the associated processes, during a seasonal cycle.

##### a. Sensitivity to heat flux

In order to understand the different mechanisms controlling SST in different regions of the North Atlantic, four numerical experiments are used to investigate the relevant precursors of wintertime SST. We define four areas in the North Atlantic roughly of  $20^{\circ}$  in longitude and  $15^{\circ}$  in latitude (Fig. 3). Three of these areas are chosen to coincide with the centers-of-action of the North Atlantic SST tripole: US, off the United States coast, GL, to the southeast of Greenland, and ST, west of the North African coast (Grötzner et al. 1998; Venzke et al. 1999). The SST tripole is the dominant pattern of SST variability associated with the North Atlantic oscillation. A fourth area covers the midlatitude eastern Atlantic (EA) and is not known for particularly strong anomalies in connection with the tripole mode. For each experiment, the scalar function  $\mathcal{J}$  is defined as area-averaged SST over the respective region [Eq. (5)].

From the ocean state reached after spinup, the integration is continued for 15 months (450 days) with the same forcing ending on day 90 of experiment year 2 (1 Apr). At this time the average SST  $\mathcal{J}$  is computed. As the mixed layer in the North Atlantic is deepest in late March the influence of entrained subsurface water on the mixed layer is expected to be greatest then. The adjoint calculation follows the forward trajectory backward in time for 15 months to 1 January of year 1. In so doing, the adjoint model calculates the sensitivity of the average SST  $\mathcal{J}$  to the ocean state (i.e., temperature, salinity, and currents) and to surface fluxes at each grid point and time step. Thus, by performing the adjoint calculation, we obtain a description of the SST sensitivity in space and

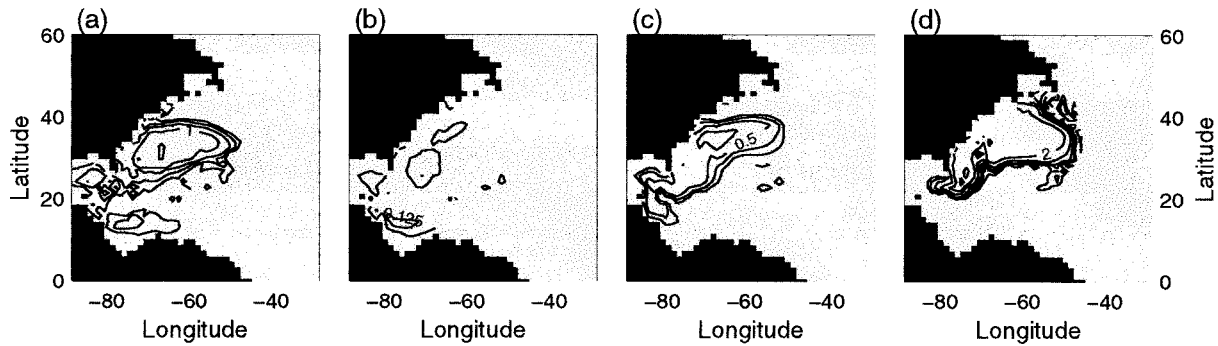


FIG. 4. Sensitivity of US averaged SST on 1 Apr year 2 (day 450) to prior air-sea heat fluxes [ $10^{-12}(\text{C s}^{-1})/(\text{W m}^{-2})$ ] on (a) 1 Apr year 1 (day 90), (b) 1 Jul year 1 (day 180), (c) 1 Oct year 1 (day 270), and (d) 1 Jan year 2 (day 360). Positive sensitivities indicate that positive heat flux anomalies warm the ocean. Contour intervals are  $\pm 0.125, 0.25, 0.5, 1, 2, 4 \times 10^{-12}(\text{C s}^{-1})/(\text{W m}^{-2})$ . Negative values have dashed contours. Sensitivities outside the selected region are negligible.

time over a 15-month period. For each experiment the SST average is defined over a different region and a separate adjoint integration is needed.

### 1) EXPERIMENT US

The sensitivity of SST in the Gulf Stream region to heat flux (expt US) at various times is shown in Fig. 4 (the following discussion considers sensitivity to heat flux at increasing lead times: that is, moving from Fig.

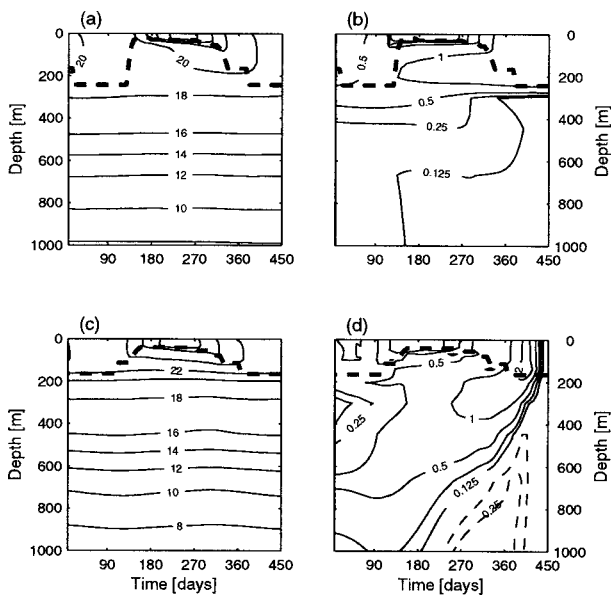


FIG. 5. Hovmöller diagrams of (a) temperature ( $^{\circ}\text{C}$ ) at  $33^{\circ}\text{N}$ ,  $64^{\circ}\text{W}$ ; (b) sensitivity ( $10^{-16} \text{ m}^{-3}$ ) of US averaged SST on 1 Apr year 2 to prior ocean temperatures at  $33^{\circ}\text{N}$ ,  $64^{\circ}\text{W}$ ; (c) temperature ( $^{\circ}\text{C}$ ) at  $31^{\circ}\text{N}$ ,  $75^{\circ}\text{W}$ ; (d) sensitivity ( $10^{-16} \text{ m}^{-3}$ ) of US averaged SST on 1 Apr year 2 to prior ocean temperatures at  $31^{\circ}\text{N}$ ,  $75^{\circ}\text{W}$ . Contour intervals for (a) and (c) are  $2^{\circ}\text{C}$ . Contour intervals for (b) and (d) are  $\pm 0.125, 0.25, 0.5, 1, 2, 4 \times 10^{-16} \text{ m}^{-3}$ . Negative values have dashed contours. The thick, dashed line indicates the depth of the mixed layer estimated as the depth at which the temperature is  $0.5^{\circ}\text{C}$  less than the surface temperature. The station locations are marked on Fig. 3. The time refers to the elapsed period since 1 Jan year 1.

4d to Fig. 4a). At a lead time of 90 days (day 360; Fig. 4d) sensitivity has traveled from the US area back up the Gulf Stream along the North American coast suggesting that advection of warm waters is the main contributor on this timescale. The positive heat flux sensitivities show that increasing (decreasing) heat flux along the Gulf Stream on 1 January year 2 increases (decreases) SST in the region US on day 450. This direct thermodynamic response makes good physical sense, although we also note there are isolated patches of negative sensitivity. In these regions (e.g., to the northeast of the primary patch) increasing heat uptake by the ocean on 1 January year 2 actually decreases the US SST 3 months later, through a dynamic (rather than kinematic) interaction that involves modified flow.

By 1 October year 1 (day 270, Fig. 4c) the sensitivity to heat flux has decreased dramatically, and the region of high sensitivity has spread farther back along the path of the Gulf Stream into the Gulf of Mexico. Three months earlier than that (1 Jul year 1, day 180, Fig. 4b) heat flux sensitivity is very weak everywhere. This means that heat flux over the North Atlantic in summer has little influence on SST in area US in the following winter. It is in accordance with the stochastic model and results by Frankignoul et al. (1998) who find a damping timescale for SST anomalies of the order of a few months. Interestingly, at lead time 1 year (1 Apr year 1), sensitivity to heat flux reappears, mainly in the southwestern part of the region US and in an area to the west of US (Fig. 4a). Although heat flux sensitivities had already propagated southward along the Florida coast and into the Gulf of Mexico by 1 October year 1, they are now concentrated in an area much closer to their origin in region US.

The reemergence of sensitivity of SST to heat flux means that heat anomalies are stored beneath the mixed layer during summer. This is confirmed by Hovmöller diagrams at locations  $33^{\circ}\text{N}$ ,  $64^{\circ}\text{W}$  (Fig. 5b) and  $31^{\circ}\text{N}$ ,  $75^{\circ}\text{W}$  (Fig. 5d). In the former, sensitivity of US SST to prior ocean temperatures is homogeneous over the upper 300 m of the water column over the 3 months of year

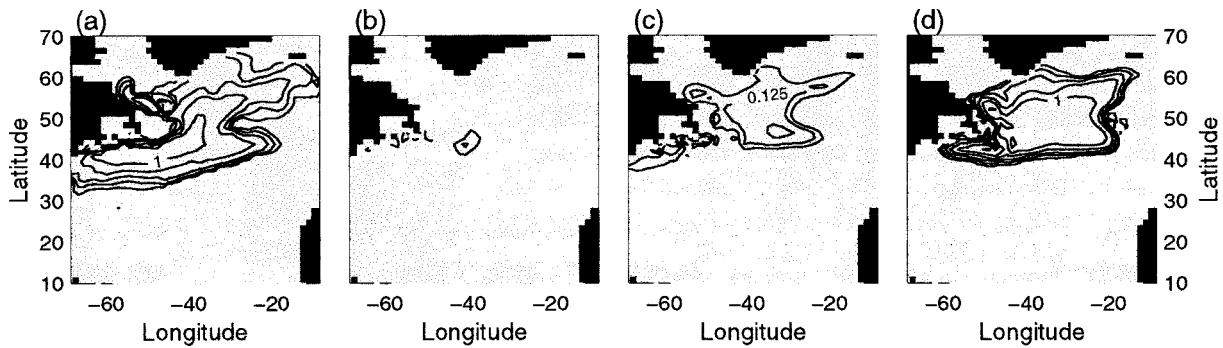


FIG. 6. Sensitivity of GL-averaged SST on 1 Apr year 2 (day 450) to prior air-sea heat fluxes [ $10^{-12}(\text{°C s}^{-1})/(\text{W m}^{-2})$ ] on (a) 1 Apr year 1 (day 90), (b) 1 Jul year 1 (day 180), (c) 1 Oct year 1 (day 270), and (d) 1 Jan year 2 (day 360). Positive sensitivities indicate that positive heat flux anomalies warm the ocean. Contour intervals are  $\pm 0.0625, 0.125, 0.25, 0.5, 1, 2, 4 \times 10^{-12}(\text{°C s}^{-1})/(\text{W m}^{-2})$  (note the additional contour lines at  $\pm 0.0625$ , in comparison to Figs. 4, 8). Negative values have dashed contours. Sensitivities outside the selected region are negligible.

2. This depth coincides with the model winter mixed layer depth at this location (shown as a dashed line in Fig. 5) confirming that vigorous mixing in winter leads to a near-surface water column that is homogeneous in sensitivity as well as temperature and salinity. Following the adjoint solution backward in time, surface sensitivity decreases rapidly to near zero during the fall of year 1. But below this shallow (30 m) layer, sensitivity retains much higher values than at the surface. An adjoint-entrainment process has sequestered sensitivity in the seasonal pycnocline where it is shielded from the ongoing memory loss at the surface. Proceeding backward through the fall and summer, sensitivity declines, at these stations, due to adjoint mixing and advection. By March year 1 (day 75), sensitivities are again homogeneous over the upper 300 m, as adjoint detrainment increases the values near the surface thereby explaining the reemergence of the signal found in Fig. 4a.

Further west of area US (Fig. 5d), sensitivity of US SST to prior ocean temperatures is near zero initially and increases at a lead time of 1–2 months due to adjoint horizontal advection of sensitivity. In other words, anomalous forcing at this location must occur no later than January–February in order to affect region US 1–2 months later. While the adjoint temperature continues to increase at a depth of 200 m, it rapidly decreases again near the surface. By April of year 1 the reemergence enhances the surface sensitivity again. This suggests, not surprisingly, that SST in US is influenced by prior SSTs upstream. At  $31^{\circ}\text{N}, 74^{\circ}\text{W}$  maximum influence from subsurface waters is 5–6 months before the calculation of the scalar function  $J$ . Interestingly, there is also a weak influence from layers below the maximum winter mixed layer (around 200 m). In fact, there is a second maximum in temperature sensitivity near 450 m during fall and summer presumably reflecting a sensitivity pathway that involves entrainment of main thermocline waters into the surface layer of region US (planetary waves are also potentially important although they

do not seem to play a role on these timescales—see sections 4d and 5).

## 2) EXPERIMENT GL

The sensitivity of SST, averaged over the region GL on 1 April year 2, with respect to prior heat flux is shown in Fig. 6. At a lead time of 3 months (Fig. 6d), the adjoint heat flux is still mostly confined to the area GL, with an indication that the signal path bifurcates and propagates back along the Gulf Stream and into the Labrador Sea. Compared to experiment US, the sensitivity is much weaker in the fall (Fig. 6c) although the two pathways to the north and the south along the western boundary can still be identified. In midbasin the sensitivity signal is advected westward along the adjoint North Atlantic Current with little propagation immediately north and south. In the spring of year 1 (day 90, Fig. 6a), sensitivities increase again, and the maximum values occur along the narrow strip of the Gulf Stream extension along  $40^{\circ}\text{N}$  into the western boundary. The influence of waters from the Labrador Sea is weaker on this timescale by a factor of 2–3.

As in experiment US, the reemergence of heat flux sensitivity is due to seasonal adjoint entrainment. Figure 7 shows Hovmöller diagrams at the surface and at 140-m depth at three different longitudes that cut through the region GL. In all of them, temperature sensitivity within the latitude band  $34^{\circ}\text{--}64^{\circ}\text{N}$  decreases rapidly near the surface and vanishes around a lead time of 6 months, whereas the subsurface values show a much slower decrease. Around day 90 the values near the surface increase again, to near the value found at 140-m depth as the mixed layer deepens through this horizon. As for experiment US, the sensitivity of SST in GL to heat flux also seems to be determined primarily by advective processes through the seasonal thermocline at least over the previous year. Propagation back along

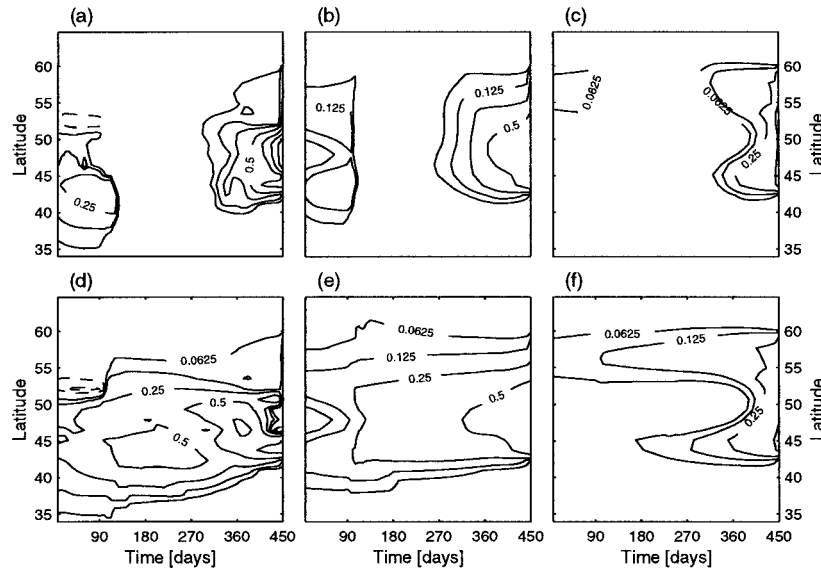


FIG. 7. Hovmöller diagrams showing the temperature sensitivity of GL-averaged SST on 1 Apr year 2 to prior ocean temperatures ( $10^{-16} \text{ m}^{-3}$ ) as a function of latitude and time since 1 Jan year 1 at 5-m depth for (a) 46°, (b) 34°, (c) 21°W; and at 140-m depth for (d) 46°, (e) 34°, and (f) 21°W. Contour intervals are  $\pm 0.0625, 0.125, 0.25, 0.5, 1, 2, 4 \times 10^{-16} \text{ m}^{-3}$ . Negative values have dashed contours. These meridional sections are shown in Fig. 3.

the North Atlantic Current and Gulf Stream is clear in Fig. 7.

3) EXPERIMENT ST

For experiment ST the annual cycle in the upper ocean is less strong. The permanent pycnocline in this area is shallow ( $\approx 100 \text{ m}$ ) and the seasonal variation in mixed layer depth is only a few tens of meters. Consequently, the sensitivity is mainly confined near the surface and damped locally over a few months. Understanding the physical processes involved in creating the sensitivity patterns is complicated by the vicinity of the equatorial current system that involves rapid currents, intense shear-flow regions and seasonal reversal of some

currents (e.g., the NECC that runs along the southern border of region ST). Fast planetary waves may also be important as van Oldenborgh et al. (1999) have shown in the Pacific. The range of mechanisms is reflected by the mesoscale patchiness we find in the patterns of sensitivity of ST-averaged SST to prior heat flux (Fig. 8).

At day 360, sensitivity has spread to the north and south of the region ST (Fig. 8d). To the north, it continues to follow the path back around the slow subtropical gyre. Initially, we find little sensitivity to the west. The currents north of 10°N are directed toward the west all year, and the only period the model NECC streams toward the east is from June to October, providing a mechanism for the influence of water masses to the west onto region ST. Indeed, in October year 1

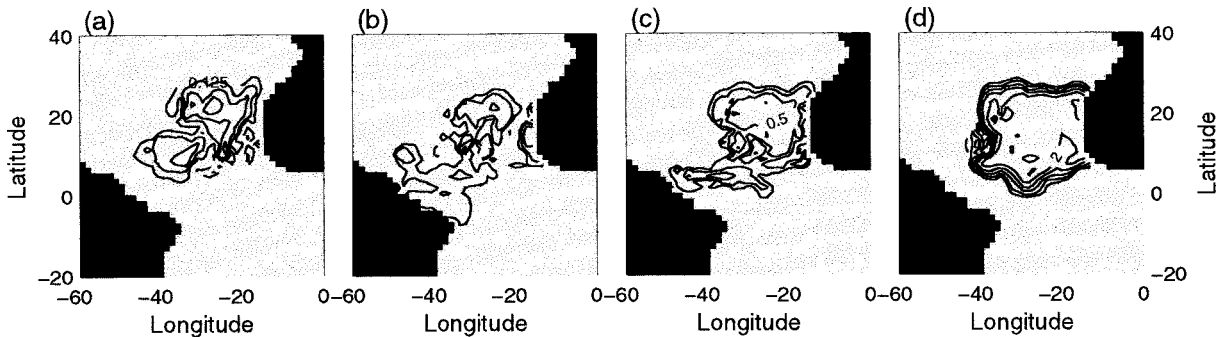


FIG. 8. Sensitivity of ST-averaged SST on 1 Apr year 2 (day 450) to prior air-sea heat fluxes [ $10^{-12} (\text{°C s}^{-1}) / (\text{W m}^{-2})$ ] on (a) 1 Apr year 1 (day 90), (b) 1 Jul year 1 (day 180), (c) 1 Oct year 1 (day 270), and (d) 1 Jan year 2 (day 360). Positive sensitivities indicate that positive heat flux anomalies warm the ocean. Contour intervals are  $\pm 0.125, 0.25, 0.5, 1, 2, 4 \times 10^{-12} (\text{°C s}^{-1}) / (\text{W m}^{-2})$ . Negative values have dashed contours. Sensitivities outside the selected region are negligible.

(day 270, Fig. 8c) the sensitivity values along  $10^{\circ}\text{N}$  have spread westward, reaching the north Brazilian coast. The influence of the adjoint North Brazil Current then spreads the sensitivity to the south along the coast by July year 1 (Fig. 8b).

In contrast to experiments GL and US, the heat flux sensitivities in summer are less strongly damped and do not then recover as much in the previous spring (day 90; Fig. 8a). In other words, heat flux perturbations can affect SST in region ST year-round although wintertime forcing is still most effective. Given the shallow mixed layers in this region and hence the rapid damping timescale, the maintenance of sensitivity through summer is interesting (days 150–250; Figs. 8b,c). The weak signal of reemergence of heat flux sensitivity (Fig. 8a) is due to the weak seasonal cycle in mixed layer depth. But interaction with mean currents and, perhaps, fast planetary waves is also important. In any event, the sensitivity dynamics of the tropical Atlantic deserve a more detailed study. Finally, note that the area reached by the heat flux sensitivity covers a larger portion of the basin compared to the influence in GL and US due to the stronger currents in the tropical Atlantic and the weaker vertical spreading of sensitivity.

#### 4) EXPERIMENT EA

Interestingly, there is no qualitative difference in the mechanisms that affect end-of-winter SST between experiment EA and experiments US and GL. The dominant sensitivity signal is a zonal band near  $40^{\circ}\text{N}$  that runs from the western edge of region EA along the model North Atlantic Current and then along the Gulf Stream, reaching  $20^{\circ}\text{N}$  along the North American coast at the beginning of year 1 (not shown). Sensitivities to heat flux show the characteristic signature of decrease, very weak values during the summer of year 1, and subsequent recovery by spring year 1. The reemergence of sensitivity indicates a zonal speed of  $0.05\text{--}0.06\text{ m s}^{-1}$  along  $40^{\circ}\text{N}$  consistent with adjoint advection in the Azores Current and North Atlantic Current. The time evolution of sensitivity of EA-averaged SST to subsurface temperatures shows the same westward propagation of the signal.

#### b. Summary of experiments: Total sensitivity of SST to prior heat flux

To summarize these results we calculate a single number from the adjoint heat flux fields—the total sensitivity. Total sensitivity of SST  $\mathcal{J}$  to heat flux  $Q$  is defined as the square root of the second raw moment of  $\partial\mathcal{J}/\partial Q$  (the Euclidean norm). This quantity has the following interpretation: given any heat flux perturbation with a specified mean and variance, the total sensitivity is the maximum (linear) response in  $\mathcal{J}$  that is possible. The total sensitivity as a function of time is shown in Fig. 9 for each experiment. For comparison, we also show

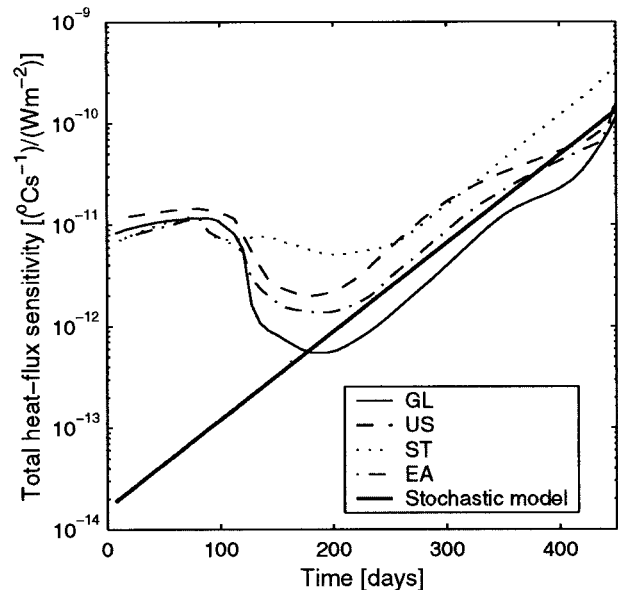


FIG. 9. Total heat flux sensitivity [ $^{\circ}\text{C s}^{-1}/(\text{W m}^{-2})$ ] as a function of time for all four experiments. Time refers to the period since 1 Jan year 1. The total heat flux sensitivity is the norm of the sensitivity pattern shown in, e.g., Fig. 4. Also shown is the sensitivity that would arise from the simple stochastic climate model assuming a mixed layer depth of 40 m. See text for details.

the graph that would result from the simple damping of SST due to negative heat flux feedback at the surface. We have chosen a damping timescale of 50 days that results from the relaxation term used in the GCM assuming a mixed layer depth of 40 m.

Initially, for all experiments but ST, the decrease in total sensitivity is rapid, considerably faster than a simple damping of SST would yield. The reason is that the mixed layer is deepest during the three months preceding the calculation of  $\mathcal{J}$ , and the influence of heat flux onto SST is reduced through vigorous mixing throughout the mixed layer. From an adjoint perspective, proceeding back in time, the sensitivity is diluted through the deep mixed layer. The value at the surface is reduced much faster, therefore, than in the simple damping formulation assuming a shallow 40-m layer. Consistent with this idea, the most rapid decrease in total sensitivity occurs in experiment GL that has the deepest winter mixed layer and greatest range of mixed layer depths (Fig. 2).

Between days 360 and 210 when the mixed layer depth decreases (going back in time), the rate of decrease in total sensitivity closely matches the slope of the simple damping scenario. In spring of year 1 (days 90–120) the sensitivity increases again, most strongly for experiments GL and US. This signature is also seen in the instantaneous plots (Figs. 4, 6, 8). For experiment ST, the reemergence signal is less pronounced in spring year 1 (Fig. 9). The fractional decrease in total sensitivity over a year is 3–4 times greater than in the other experiments mainly due to weaker vertical spreading of

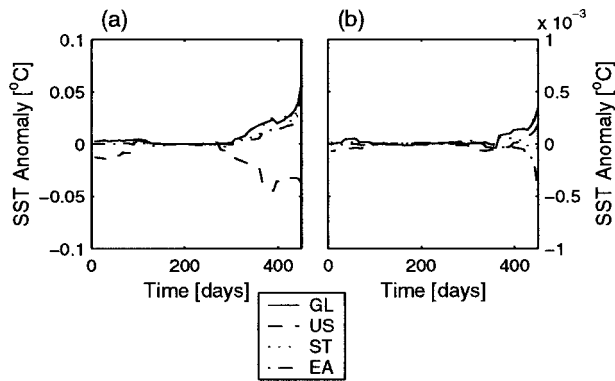


FIG. 10. Model SST anomalies ( $^{\circ}\text{C}$ ) caused by prior forcing anomalies. The first EOF of (a) climatological heat flux variability and (b) climatological wind stress variability is projected onto SST sensitivity for 1 month. The subsequent end-of-winter (day 450) SST anomaly in the four experiments is shown. See text for details.

sensitivity in the subtropics and Tropics. Overall, the different graphs suggest that wintertime SSTs in the areas GL, US, and EA are somewhat influenced by air-sea heat fluxes in the preceding winter—the total sensitivity is 10 times smaller on 1 April year 1 than it is a year later. In the subtropics (expt ST) this pathway via the seasonal thermocline is less effective. The weaker penetration of sensitivity into the main thermocline does prolong the memory of prior heat fluxes, however, and there is a smaller difference between winter and summer sensitivities.

#### c. Projection of climatological variability: Model SST anomalies caused by prior heat flux anomalies

Finally, we estimate the actual SST change that would occur in the GCM given a realistic heat flux anomaly. To do so we project the heat flux sensitivity fields onto realistic climatological perturbations of heat flux derived from observations. To find a typical spatial pattern of heat flux anomaly  $\Delta Q$ , we apply empirical orthogonal function (EOF) analysis to the net air-sea heat flux derived from the da Silva dataset (1945–93; daSilva et al. 1994). The typical pattern for the winter months (first EOF, not shown) has a similar structure to the SST tripole, consisting of three antinodes over the North Atlantic. It retains its structure through the winter (Nov–Mar). In summer the pattern shifts considerably to the north and weakens. For every month, we use this EOF and project it onto the sensitivity field using (6) assuming the heat flux anomaly persists for 1 month (Fig. 10a). We interpret the sign of the SST anomaly as follows: a wintertime heat flux perturbation with the tripole pattern and negative anomalies off the North American coast and positive anomalies over areas GL and ST gives negative SST anomalies in US and positive SST anomalies in GL and ST on 1 April year 2. Hence, as discussed in section 4a, SST responds to anomalous heat fluxes with a local perturbation of the expected sign.

In contrast to the evolution of the total sensitivities, the actual SST anomalies are comparable in magnitude for years 1 and 2, at least for experiment US (Fig. 10a). This is because there is a greater projection of the heat flux patterns on the sensitivity fields in year 1, when they have grown in scale, than in year 2. This effect compensates the reduced sensitivity amplitudes and gives SST anomalies that are 3–30 times smaller for winter year 1 than 1 April year 2. The anomalies are very weak during spring and summer reflecting the lower total sensitivity at this time as explained in sections 4a and 4b. The reduced amplitudes of the heat flux EOFs in these months also contribute, however. In this sense, the forcing variability is well-matched to the ocean dynamics because the peak heat flux variance occurs in winter when the ocean is most sensitive to it.

It is interesting that the summer SST anomaly in experiment ST is similar to the other experiments despite stronger total sensitivities for experiment ST. The reason is the heat flux variability at this site is relatively weaker in summer. Also note that the projection onto the adjoint sensitivities typically results in the lowest SST anomaly in region EA. As we find no evidence for different mechanisms in this region, this result suggests that the tripole mode is determined by the atmospheric heat flux patterns rather than the result of oceanic dynamics, at least on interannual timescales.

#### d. Sensitivity to wind stress and freshwater flux

The results of the sensitivity calculations indicate that wind stress is  $O(100)$  times less effective at influencing SST over 15 months than heat flux (Fig. 10b). The wind stress EOFs were calculated in the same way as those of  $\Delta Q$ , for each month separately. The first EOF is a basin-scale cyclone over the North Atlantic, associated with the negative phase of the North Atlantic oscillation, which shifts north-southward during the seasonal cycle. The projection of this pattern gives the largest SST anomalies (compared to the higher-order EOFs) for all four experiments, and is shown in Fig. 10b. In summer year 1 (days 100–300) both wind stress and heat flux-induced SST anomalies are much weaker with somewhat less seasonality in the wind stress sensitivity. Again, there is no qualitative difference for experiment EA.

Lower wind stress-induced SST anomalies occur partly because wind stress does not directly affect temperature (via a thermodynamic process) and partly because there is a weak projection of the atmospheric wind stress variability onto the sensitivities. Wind stress sensitivities are more long-lived than heat flux sensitivities, however, as there is no damping air-sea feedback on surface flow anomalies due to wind stress fluctuations. The wind is also more able to excite interior temperature anomalies (planetary waves), which are not strongly damped, and this process can occur throughout the year. We expect wind stress to become progressively more

important further back in time because heat flux sensitivity will steadily fall and wind stress sensitivities will move upscale and hence have a larger projection on the wind stress EOFs. Investigation of sensitivities on longer timescales with longer adjoint calculations is ongoing.

Our adjoint calculations also provide the sensitivity of SST to freshwater forcing. Changes in evaporation and rainfall can, in principle, play an important role through modified geostrophic advection and mixed layer dynamics. Over the seasonal cycle these experiments suggest they are negligible compared to heat flux perturbations, however. The peak SST anomalies due to freshwater changes are  $O(10^5)$  times smaller than actual heat flux sensitivity (not shown).

#### e. Importance of nonlinearity

The relevance of our results to the full GCM (and the real ocean) depends on the validity of the linearization of the model equations. An important issue is whether the adjoint sensitivities are a good approximation to finite-amplitude sensitivities that may also involve nonlinear processes. Experiments using the GCM in which some of the control variables have been perturbed provide a direct check of the importance of nonlinearity on the timescales we consider here.

We perturb the heat flux forcing fields  $Q$  and integrate the GCM forward in time to calculate  $j$ . The change  $\Delta j$  between the unperturbed and the perturbed integration is then compared to the adjoint estimate  $\langle \nabla, j, \Delta Q \rangle$ , which is only accurate to first order. For experiment US, we start the forward calculation at the beginning of year 2, adding a perturbation to the heat flux upstream of the area where the average SST is calculated ( $23^\circ$ – $32^\circ$ N,  $79^\circ$ – $74^\circ$ W). The adjoint sensitivity in this area is about  $2.1 \times 10^{-12} \text{ }^\circ\text{C s}^{-1}/(\text{W m}^{-2})$  (Fig. 4). This means that, if  $\Delta Q$  is  $1 \text{ W m}^{-2}$  at one such grid point for 1 time step (4 h) at this time, the expected US-average-SST change three months later is around  $3.0 \times 10^{-8} \text{ }^\circ\text{C}$ . We add perturbations of 50 and  $\pm 100 \text{ W m}^{-2}$  for 1 week at 33 grid points. The results of the perturbation experiments are summarized in Table 1 and show that the GCM response is almost linear. For typical heat flux fluctuations of  $50 \text{ W m}^{-2}$ , the quadratic  $\Delta Q$  term in a Taylor-series expansion of  $j$  is just 0.1% of the linear term. The finite-amplitude sensitivities are 10% smaller than the infinitesimal sensitivity (from the adjoint), however. This difference arises because the adjoint model is not exact. Various minor compromises are made in constructing the adjoint software so as to derive a stable, efficient code. There is a concomitant loss of accuracy although we believe this is an acceptable price to pay. Numerical error in the adjoint calculation may also play a role (Sirkes and Tzipermann 1997 discuss aspects of this issue). When the perturbations are applied at the beginning of year 1, the quadratic  $\Delta Q$  term is about 10% of the linear term. In this case, the adjoint sensi-

TABLE 1. Comparison of heat flux sensitivities for expt US, derived from finite-amplitude perturbations of the GCM and the adjoint. The Gulf Stream heat flux perturbation  $\Delta Q$  is applied for 1 week to 58 grid cells around  $30^\circ$ N at the beginning of year 1 (day 1) and to 33 grid cells around  $25^\circ$ N at the beginning of year 2 (day 361). The resulting change in US-averaged SST is  $\Delta j$ , as computed by the full GCM. Also shown is the sensitivity  $\delta j$  derived from the adjoint model [see Eq. (6)].

Start of perturbation (day)	$\Delta Q$ ( $\text{W m}^{-2}$ )	$\Delta j$ ( $\times 10^{-3} \text{ }^\circ\text{C}$ )	$\delta j$ ( $\times 10^{-3} \text{ }^\circ\text{C}$ )
1	0	0	0
	-50	-2.14	-1.77
	100	3.62	3.54
	-100	-5.14	-3.54
361	0	0	0
	50	1.88	2.08
	100	3.83	4.16
	-100	-3.81	-4.16

tivity is about 4% larger than the finite-amplitude sensitivity. This weak nonlinearity encourages us to believe the adjoint sensitivities accurately reflect the finite-amplitude sensitivities of the GCM. The issue of unrepresented chaotic processes in the GCM is addressed in the next section.

## 5. Summary and discussion

We use the adjoint of an ocean GCM to estimate (linear) sensitivities of North Atlantic SST to prior surface fluxes and the ocean state. As outlined in section 2, we can discuss the results using qualitatively familiar “adjoint mechanisms” that identify linear causal chains in the system. This nontrivial property of the sensitivity dynamics is a remarkable consequence of the bilinear identity (7) and applies in general. Indeed, the adjoint sensitivity method has great potential for diagnosing mechanisms in climate models. By calculating adjoint sensitivities we also obtain quantitatively significant results, at least in the context of the current GCM.

The results of this study show that end-of-winter SSTs are mainly determined by local, contemporaneous heat fluxes. This finding is consistent with the scaling arguments of Gill and Niiler (1973) and the climatological analysis of Cayan (1992). Our GCM includes an SST relaxation with a coefficient of  $40 \text{ W m}^{-2} \text{ }^\circ\text{C}^{-1}$  to represent the negative feedback of heat fluxes and SST. This parameterization has been widely used in ocean GCMs and constitutes the essence of the simple Frankignoul and Hasselmann (1977) stochastic model. Our results show that, even in regions of moderately strong flow, the exponential loss of heat flux memory predicted by the stochastic model still basically applies. The influence of heat flux one year ahead is substantially underestimated by the simple stochastic model, however. Mixed layer thermodynamics provide a memory pathway via the seasonal thermocline, that prolongs the influence of fluxes beyond the stochastic-damping time-

scale. For end-of-winter SST, and realistic spatial forcing patterns, the influence of the previous winter's heat flux is 3–30 times less strong than the contemporaneous forcing in the SST-tripole antinodes (Fig. 10a).

This modest influence of prior heat fluxes may underestimate their true importance. One reason is that the present model of sensitivity damping treats all scales equally. In reality, larger SST anomalies are relatively more persistent (Frankignoul et al. 1998). This effect will tend to make earlier heat fluxes more important as the SST-sensitivity patterns grow in scale proceeding backward in time (as can be seen in Figs. 4, 6, and 8). To account for this effect, a scale-selective SST damping is required, of the kind used by Chen and Ghil (1996) or Rahmstorf and Willebrand (1995), for example. Another, related, reason is that the scales of air–sea heat flux variability are not well-matched to the scales of sensitivity. In other words, the EOFs of heat flux variance do not project strongly onto the sensitivity patterns. Proceeding backward in time involves an upscale spread in sensitivity and thus a stronger projection, however. Earlier heat flux anomalies may therefore be progressively more influential on SST than extrapolating our current results suggests. In any event, investigation of the impact of alternative formulations of the air–sea flux feedback is needed. Ideally, the ocean GCM would be coupled to a deterministic model of low-frequency atmospheric variability to study the sensitivity dynamics of the ocean–atmosphere system as a whole. Such investigations are underway.

Our present results may also inaccurately estimate the importance of earlier heat fluxes because the GCM and adjoint model do not contain a chaotic mesoscale eddy field. Including eddies in the GCM would cause the adjoint sensitivity fields to grow exponentially backward in time as discussed in section 2. In practice, the nonlinear eddy interactions would halt the exponential growth, although these dynamics are not captured by the adjoint sensitivity method [Lea et al. 2001, unpublished manuscript] and Lea et al. (2000) discuss this issue in detail]. Nevertheless, to the extent that the overall effect of eddies is accurately parameterized by our subgrid-scale closure scheme, the present sensitivity results are robust. Our tacit assumption is that the unpredictable eddy interactions do not dominate the sensitivity dynamics or large-scale SST variability. We anticipate that the primary mechanisms influencing SST that we identify here would still apply in GCMs with resolved mesoscale variability and in the real ocean. We also note that, even if this is not the case, our results do apply to the class of models currently used for climate studies (which do not resolve eddies). They are also relevant to recent theories of low-frequency coupled variability that do not invoke chaotic eddy mechanisms (e.g., Grötzner et al. 1998; Marshall et al. 2001).

We use an ocean GCM in this study, but, to some extent, our results can be understood with a one-dimensional model of the mixed layer and seasonal ther-

mocline. The important thermodynamics for the re-emergence signals are captured in the cycle of summer stratification and winter mixing. The advective signals (cf., e.g., Figs. 4b and 4c) can only be modeled by a three-dimensional dynamical model, however. Also, the potential importance of wave processes requires a GCM. Our results suggest that the influence of wind stress on SST (and hence the role of planetary waves) is  $O(100)$  times smaller than heat flux with lead times up to 15 months (cf. Figs. 10a and 10b). Several studies suggest that wind stress anomalies and planetary wave propagation are important on the decadal timescale, however (Grötzner et al. 1998; Frankignoul et al. 1997). Although wind stress affects SST indirectly (i.e., via adiabatic processes), we anticipate that prior wind stress anomalies will become progressively more important compared to heat flux anomalies at longer lead times. Clearly, the full primitive equations, rather than a one-dimensional mixed layer model, are needed for studies of this type.

Over periods near a decade subduction and gyre-scale transport of mode-water anomalies may also become important. Our sensitivity experiments only show the final stages of this process as thermocline waters are entrained into the Gulf Stream mixed layer, for example (expt US; see Fig. 5d). We are now extending our sensitivity calculations to investigate the relative importance of mode-water anomalies compared to planetary wave signaling. On timescales of several decades, thermohaline processes are likely to be important too, perhaps driven by fluctuations in freshwater delivery to the subpolar North Atlantic (Rahmstorf, 1996).

Finally, comparison of experiment EA with the others shows that there is no inherently oceanic reason why EA is unimportant in the SST tripole. The same sensitivity pathways apply to the antinodes of the tripole pattern (expts US, ST, and GL) although there are some quantitative differences (Fig. 10). There is also no indication of correlation between regions GL and ST or anticorrelation with region US. These findings therefore reinforce the picture that the SST tripole is primarily a local, recent oceanic response to heat flux forcing by the atmosphere (Cayan, 1992; Seager et al. 2000). Although interior ocean processes have some influence over a seasonal cycle, the dominant interaction seems to be an ocean response to atmospheric forcing on this timescale.

*Acknowledgments.* We thank Andreas Sterl for providing the Atlantic version of HOPE and Geert-Jan van Oldenborgh for generous assistance with the adjoint of the HOPE model. Myles Allen helped design the experimental strategy. The Tangent-Linear and Adjoint Model compiler (Giering and Kaminski, 1998) was very useful in deriving the adjoint model. The Natural Environment Research Council of the United Kingdom supported this study (GR3/11177, GST/02/2865).

## REFERENCES

- Alexander, M. A., and C. Deser, 1995: A mechanism for the recurrence of wintertime SST anomalies. *J. Phys. Oceanogr.*, **25**, 122–137.
- Cacuci, D. G., 1981: Sensitivity theory for non-linear systems. 1. Non-linear functional-analysis approach. *J. Math. Phys.*, **22**, 2794–2802.
- Cayan, D. R., 1992: Latent and sensible heat flux anomalies over the northern oceans: Driving the sea surface temperature. *J. Phys. Oceanogr.*, **22**, 859–881.
- Chen, F., and M. Ghil, 1996: Interdecadal variability in a hybrid coupled ocean–atmosphere model. *J. Phys. Oceanogr.*, **26**, 1561–1578.
- daSilva, A., A. C. Young, and S. Levitus, 1994: *Algorithms and Procedures*. Vol. 1, *Atlas of Surface Marine Data 1994*, NOAA Atlas NESDIS, 83 pp.
- Errico, R. M., 1997: What is an adjoint model? *Bull. Amer. Meteor. Soc.*, **78**, 2576–2591.
- Esbensen, S. K., and Y. Kushnir, 1981: The heat budget of the global ocean: An atlas based on estimates from surface marine observations. Oregon State University Tech. Rep. 29, Climate Research Institute, 27 pp.
- Farrell, B. F., and P. J. Ioannou, 1996: Generalized stability theory. Part I: Autonomous operators. *J. Atmos. Sci.*, **53**, 2025–2040.
- Frankignoul, C., 1985: Sea surface temperature anomalies, planetary waves and air–sea feedback in the middle latitudes. *Rev. Geophys.*, **23**, 357–390.
- , and K. Hasselmann, 1977: Stochastic climate models. Part II. Application to sea-surface temperature anomalies and thermocline variability. *Tellus*, **29**, 289–305.
- , P. Müller, and E. Zorita, 1997: A simple model of decadal response of the ocean to stochastic wind stress forcing. *J. Phys. Oceanogr.*, **27**, 1533–1546.
- , A. Czaja, and B. L'Heveder, 1998: Air–sea feedback in the North Atlantic and surface boundary conditions for ocean models. *J. Climate*, **11**, 2310–2324.
- Giering, R., and T. Kaminski, 1998: Recipes for adjoint code construction. *ACM Trans. Math. Software*, **24**, 437–474.
- Gill, A. E., and P. P. Niiler, 1973: The theory of the seasonal variability in the ocean. *Deep-Sea Res.*, **20**, 141–177.
- Gordon, C., C. Cooper, C. A. Senior, H. Banks, and R. Woods, 2000: The simulation of SST, sea ice extents and ocean heat transports in a version of the Hadley Centre coupled model without flux adjustments. *Climate Dyn.*, **16**, 147–168.
- Grötzner, A., M. Latif, and T. P. Barnett, 1998: A decadal climate cycle in the North Atlantic Ocean as simulated by the ECHO coupled GCM. *J. Climate*, **11**, 831–847.
- Hasselmann, K., 1976: Stochastic climate models. Part I. Theory. *Tellus*, **28**, 473–485.
- Hellermann, S., and M. Rosenstein, 1983: Normal monthly wind stress over the world ocean with error estimates. *J. Phys. Oceanogr.*, **13**, 1093–1104.
- Jaeger, L., 1976: Monatskarten des Niederschlags für die ganze Erde. Ber. des Deutschen Wetterdienstes Tech. Rep. 139 (Band 18), Offenbach, Germany, 33 pp.
- James, I. N., and P. M. James, 1989: Ultralow-frequency variability in a simple circulation model. *Nature*, **342**, 53–55.
- Lanczos, C., 1961: *Linear Differential Operators*. Dover, 576 pp.
- Latif, M., and T. P. Barnett, 1996: Decadal variability over the North Pacific and North America: Dynamics and predictability. *J. Climate*, **9**, 2407–2423.
- , K. Arpe, and E. Roeckner, 2000: Oceanic control of decadal North Atlantic sea level pressure variability in winter. *Geophys. Res. Lett.*, **27**, 727–730.
- Lea, D. J., M. R. Allen, and T. W. N. Haine, 2000: Sensitivity analysis of the climate of a chaotic system. *Tellus*, **52A**, 523–532.
- Levitus, S., 1982: *Climatological Atlas of the World Ocean*. NOAA Prof. Paper 13, 173 pp.
- Marotzke, J., R. Giering, K. Q. Zhang, D. Stammer, C. Hill, and T. Lee, 1999: Construction of the adjoint MIT ocean general circulation model and application to Atlantic heat transport sensitivity. *J. Geophys. Res.*, **104**, 29 529–29 547.
- Marshall, J. C., A. J. Nurser, and R. G. Williams, 1993: Inferring the subduction rate and period over the North Atlantic. *J. Phys. Oceanogr.*, **23**, 1315–1329.
- , H. Johnson, and J. Goodman, 2001: A study of the interaction of the North Atlantic oscillation with ocean circulation. *J. Climate*, **14**, 1399–1421.
- Morse, P. M., and H. Feshbach, 1953: *Methods of Theoretical Physics*. McGraw-Hill, 1008 pp.
- Palmer, T. N., 1996: Predictability of the atmosphere and oceans: From days to decades. *Decadal Climate Variability*, D. L. T. Anderson and J. Willebrand, Eds., NATO ASI Series, Vol. I 44, Springer, 493 pp.
- Rahmstorf, S., 1996: On the freshwater forcing and transport of the Atlantic thermohaline circulation. *Climate Dyn.*, **12**, 799–811.
- , and J. Willebrand, 1995: The role of temperature feedback in stabilizing the thermohaline circulation. *J. Phys. Oceanogr.*, **25**, 787–805.
- Seager, R., Y. Kushnir, M. Visbeck, N. Naik, J. Miller, G. Krahnmann, and H. Cullen, 2000: Causes of Atlantic Ocean climate variability between 1958 and 1998. *J. Climate*, **13**, 2845–2862.
- Sirkes, Z., and E. Tzipermann, 1997: Finite difference of adjoint or adjoint of finite difference? *Mon. Wea. Rev.*, **125**, 3373–3378.
- Smith, L. A., C. Ziehmann, and K. Fraedrich, 1997: Uncertainty dynamics and predictability in chaotic systems. *Quart. J. Roy. Meteor. Soc.*, **123**, 1–34.
- Sutton, R. T., and M. R. Allen, 1997: Decadal predictability of Gulf Stream SSTs. *Nature*, **388**, 563–567.
- van Oldenborgh, G. J., G. Burgers, S. Venkze, C. Eckert, and R. Giering, 1999: Tracking down the ENSO delayed oscillator with an adjoint OGCM. *Mon. Wea. Rev.*, **127**, 1477–1496.
- Venkze, S., M. R. Allen, R. T. Sutton, and D. P. Rowell, 1999: The atmospheric response over the North Atlantic to decadal changes in sea surface temperature. *J. Climate*, **12**, 2562–2584.
- Watanabe, M., and M. Kimoto, 2000: On the persistence of decadal SST anomalies in the North Atlantic. *J. Climate*, **13**, 3017–3028.
- Wolff, J.-O., E. Maier-Reimer, and S. Legutke, 1997: The Hamburg Ocean Primitive Equation model HOPE. Deutsches Klimarechenzentrum Tech. Rep., Hamburg, Germany, 98 pp.